13

Production of ultra-thin superconducting films from NbN by cathode sputtering at substrate temperatures 20 °C–120 °C

© B.A. Gurovich,[1] B.V. Goncharov,[1] K.E. Prikhodko,[1,2] V.L. Stolyarov,[1] L.V. Kutuzov,[1]
D.A. Goncharova,[1] E.M. Malieva,[1] M.M. Dementyeva,[1] G.Yu. Golubev,[1] A.S. Frolov[1]

[1]National Research Center „Kurchatov Institute“,
123098 Moscow, Russi
[2]Research Nuclear University „MEPhI“,
115409 Moscow, Russia
e-mail: goncharov_bv@nrcki.ru

Received May 12, 2025
Revised May 12, 2025
Accepted May 12, 2025

Ultrathin NbN films with a thickness of 5.5 nm were made by cathode sputtering. The films were sputtered on sapphire substrates at various temperatures from 20 °C to 120 °C. The transition temperature to the superconducting state, depending on the substrate temperature during sputtering, was 6.9−9.8 K. The technique of sputtering ultrathin NbN films using cathode sputtering (Penning cells) is described in detail. The critical current density of the studied films lies in the range of $1.12-3.5\,10^5$ A/cm^2.

Keywords: cathodic sputtering, niobium nitride, inhomogeneity, transition temperature to the superconducting state, critical current density

DOI: 10.61011/TP.2025.10.62083.111-25

Introduction

Ultrathin niobium nitride (NbN) films are among the most widely used and highly-demanded materials in terms of superconductivity. Due to a high critical superconducting transition temperature T_C (up to 17 K), high critical current densities (J_C) up to 10 MA/cm^2 (generally for films with thicknesses of 50 nm and more made at high temperatures), chemical stability and thermal cycling resistance, NbN films hold a prominent place in current research and applications in the field of superconducting electronics. They are used to make a wide range of superconducting electronic devices: superconducting single-photon detectors, photon number resolution detectors [1,2], hot electron bolometers [3,4], logical devices designed for various applications [5–7], Josephson junctions [8,9], etc. To date, many techniques have been developed for fabricating thin and ultrathin NbN films having high electrophysical characteristics. Note that the properties of films grown using various techniques are significantly affected by three factors: wafer material, active gas mixture components, and wafer temperature during deposition (deposition temperatures are generally relatively high: 300 °C–1000 °C).

Atomic layer deposition (ALD) process compared with most other techniques provides the most accurate control over the desired film thickness during growth because a consecutive layer-by-layer and self-limiting chemical process is used. The disadvantages of the process may include high cost (due to employment of expensive precursors) and relatively slow growth rate. Results of NbN film growth using the ALD technique are reported in [10–17]. Thus, in [10], 50 nm films were grown on sapphire wafers at a wafer temperature of 570 K (followed by annealing at 970, 1050 K and without annealing) and a superconducting transition temperature of 12.35 K. Results for films on high-resistance silicon wafers are reported in [11]. Wafer temperatures were 250 °C to300 °C. Film thicknesses were within 4−30 nm, and T_C was within 7.5−10.9 K, respectively. Work [12] used the PEALD (plasma-enhanced atomic layer deposition) technique. Films were deposited onto SiO_2 and Si wafers at temperatures ranging from 100 °C to300 °C. The authors successfully achieved T_C 6.4−13.7 K at film thicknesses of 22−37 nm. The authors of [13] also used the PEALD technique and demonstrated T_C 13.3 K at a wafer T of 300 °C and NbN film thickness of 61 nm. In [15], a $\sim$ 5 nm film with T_C 14.5−15 K and thickness scatter about 10 % was fabricated on a wafer with a diameter of 100 mm.

Another widely used NbN film deposition technique is pulsed laser deposition (PLD). PLD NbN films generally have a very high quality with recorded T_C up to 15.2 K [17] (with thicknesses of 50 nm). Results for various types of wafers have been obtained in this area [17,18]. Typical wafer temperature for this technique is 400 °C to800 °C [19,20]. Disadvantages of this method include high quality target feedstock requirements.

Ultrathin NbN films are rarely produced using a chemical vapor deposition (CVD) technique. Advantages of this technique include a relatively low cost and ability to vary the structures of resulting NbN films depending on the wafer temperature [21,22]. For films deposited by this method, the highest T_C up to 17.06 K [23] was recorded at a film thickness of 50 nm. Disadvantages include high process

temperatures (900 °C to1300 °C) that limit compatibility with many processes used for manufacturing nanoscale superconductor devices.

One of the most widely used methods for ultrathin NbN film growth is magnetron sputtering. To date, a lot of data have been obtained concerning the properties of ultrathin NbN films produced using this technique [22,24–29]. Both DC sputtering [22,24–29], and RF sputtering [22] processes are suitable. Advantage of the technique include high performance (compared with other techniques), relatively low cost (of both equipment and consumables) and coverage of large areas [30]. Magnetron sputtering requires concerted and accurate control of a set of sputtering process variables (relations between partial gas pressures and discharge parameters that may vary during sputtering) [31–33]. Relatively high wafer temperature is also generally required (350 °C to 600 °C).

Wafer material is an important factor affecting the final properties of NbN films. In [22,24–36], NbN films are deposited onto various types of wafers (Al_20_3, 3C-SiC/Si, SiO_2, MgO). The authors of [24,25] used sapphire heated to 600 °C as wafers for deposition of 4.4 nm NbN films with a transition temperature of T_C 13.3 K. Also in [26], 5 nm NbN films deposited onto Si (T_C 9.5 K) were compared with 4 nm films deposited onto a 3C-SiC buffer layer (T_C 11.8 K). MgO used as a wafer material in [27,28] has shown better results at lower heating temperatures (400 °C) with a film thickness of 7 nm and transition temperature of T_C 13.7 K. Summing up, it may be said that Al_2O_3 and MgO shall be the considered as the most preferable wafer materials. Sputtering techniques and specifications of ultrathin NbN films are summarized in Table 1.

The authors of this work introduce an ultrathin niobium nitride film fabrication technique using ion-beam target sputtering in the „Penning cell“. The proposed deposition method combines the advantages of the above-mentioned methods such as relatively low cost and high level of film thickness control. The proposed technique also provides control of temperature distribution over the wafer directly during sputtering to ensure high homogeneity of properties of the resulting NbN coating.

1. Description of the technique and system

Besides the magnetron, sputtering method using the Penning cell is an ion-beam sputtering alternative for growing superconducting NbN films. This technique has a system configuration concept similar to magnetron, including cathode-targets arranged in pairs with respect to a ring anode, electric and magnetic fields, gas medium with active and reactive gas combination. National Research Center „Kurchatov Institute“ has developed this technique for deposition of various thin layers (for example, diamond-like carbon films) [37]. A group of authors designed and fabricated a system that used this concept. System was called the UIR-11 Ion-Beam Sputtering System.

The concept involves plasma generation by longitudinal and partially crossed magnetic and electric fields due to physical processes equivalent to a magnetron. Magnetic field is produced by DC-carrying solenoids that were equipped by a cooling water circuit for cooling. Plasma discharge initiation is followed by bombardment of cathode-targets (Nb) with active gas (Kr), which results in knocking Nb atoms off the cathode surface. Under the action of electric and magnetic field, electrons support glow discharge. Simultaneously, reactive gas, N_2, is injected into the volume. Molecules of this gas pass into an excited state within plasma and further interact on the wafer surface (on the holder between cathodes) to form NbN with deposited Nb atoms. Such configuration uses increased (with respect to magnetron) discharge voltage from hundreds volts (as in magnetron) to several kilovolt (in our case $3-4$ kV). But the Penning discharge current (~ 2 mA) and the neutral gas pressure (initial pressure is generally equal to $7-8\cdot10^{-8}$ Torr, operating pressure is $\sim 5-6\cdot10^{-5}$ Torr) are much lower than those in the magnetron discharge. Due to a higher energy of cathode-bombarding ions, sputtered atoms have a mean energy that is much higher than that in magnetron. Performance of the method is lower than in the magnetron (typical sputtering rate is 0.81 nm/min), due to which it is possible to considerably improve the deposited film thickness control.

From a practical standpoint, principle of sputtering using the Penning cell has a set of differences from the magnetron version, i.e:

— plasma is produced in longitudinal magnetic and electric fields and magnetic and electric fields locally crossed near the anode (magnetron has crossed fields), which provides a longer electron path in the discharge and makes it possible to increase the bombarding ion energy, which in turn requires higher voltages for discharge:

— the technique prevents from using a gateway and quick replacement of deposited samples. Wafer replacement requires opening of the active volume to atmosphere, which decelerates the process as a whole, but is beneficial to quality and stability of film properties. Deposited material is accumulated on the magnetron chamber walls and, without cyclic atmosphere admissions, considerably changes the active gas mixture composition, therefore, the gas mixture shall be continuously monitored and adjusted. Nevertheless, the UIR-11 is designed to accommodate up to six sampler holders (three holders on each side, vertically with respect to each other) and to perform consecutive sputtering in one charge. The configuration also implies employment of up to three various materials for sputtering in the form of sets of cathodes. Cathode and anode pairs are insulated from each other. High voltage inputs and solenoids are separated and controlled by independent power sources. Thus, several layers of various materials may be deposited onto a single sample or a single material may be deposited simultaneously onto several samples in a single charge. These functions

Table 1. Specifications of NbN films grown using various methods

Film growth technique	wafer material	Wafer heating temperature, °C	Layer thickness, nm	T_C, K	Reference
PLD	MgO	600	240	16.3	[18]
	MgO	600	30	13.7	[14]
	Al_2O_3	600	200	15.5	
	Si	600	20	10.8	
	$Al_2O_3 - NbN - NiCu$	600	170	16.6	
	MgO	600	110	16.1	[20]
	Fused silica	600	110	11.8	
ALD	$SiO_2 + SiN$	300	61	13.3	[12]
	Si	250	5	7.5	[13]
	Si	250	10	9.1	
	Si	250	15	9.5	
	Si	250	20	9.7	
	Si	300	5	8.5	
	Si	300	~ 12.5	10.5	
	Si	300	~ 18	10.9	
	Si	300	25	10.7	
	Al_2O_3	297 (570 K) + annealing1050 K	50	11.91	[10]
	Al_2O_3	297 (570 K) + annealing970 K	50	12.12	
	Al_2O_3	297 (570 K)	50	12.35	
	SiO_2	600	4.4	11.3	[14]
	SiO_2	350	28	14	[16]
CVD	Al_2O_3	1300	49	16.8	[22]
	Al_2O_3	1300	49	17.02	
	$Al_2O_3 + 80$ nm AlN	1300	49	17.06	

neutralize low performance of the method compared with the magnetron;

— the techniques have considerably different cathode burning patterns, which also requires due consideration because the discharge properties are changed. In contrast to the magnetron where plasma resides mainly in the cathode space, in our case plasma in the intercathode space transforms into a streamer and is focused near the centers of cathodes (Figure 1).

Advantages of the technique include:

— relative simplicity and low cost;

— film quality may be higher compared with the magnetron due to the fact that the background vacuum in the sputtering zone weakly depends on gas exchange on the chamber walls because there is no growing film of the deposited material on the walls;

— the Penning discharge method has an optimum relation between N_2 and inert gas concentrations that is considerably higher than in the magnetron discharge case. This suggests that N_2 molecule activation efficiency is lower. But this simultaneously reduces the method sensitivity to the required stability of this relation. As shown above, when NbN films are deposited, the wafer temperature and uniform temperature distribution over the wafer are important factors influencing the film quality and properties. In the range from 20 °C to200 °C, temperature considerable affects the process result (see Section 2). For thorough temperature monitoring, a special sample holder was designed (Figure 2). The holder consists of a grounded housing that encloses a silicon carbide heating element. The heater size (18×30 mm) provides a uniform sample heating level throughout the sample area. The heater is

Table 1. (*Continuation*)

Film growth technique ReferenceT_C	wafer material	Wafer heating temperature , °C	Layer thickness, nm	, K	
Magnetron	Al_2O_3	850	20	9.5	[23]
	Si	850	20	7.2	
	SiO_2	850	20	7.7	
	Si_3N_4	850	20	7	
	Al_2O_3	850 + annealing1000 °C 20 min	20	13.5	
	Si	850 + annealing1000 °C 20 min	20	12.5	
	SiO_2	850 + annealing1000 °C 20 min	20	13.3	
	Si_3N_4	850 + annealing1000 °C 20 min	20	–	
	Al_2O_3	600	4.4	13.3	[24]
	Al_2O_3	600	4.35	13.2	[25]
	Al_2O_3	600	2.86	11.7	
	Si	800	5	9.5	[26]
	Si + 3C−SiC	800	4	11.8	
	MgO	400	7	13.7	[28]
	MgO	400	5.5	11.2	
	MgO	400	4	10.2	
	MgO	400	3	8.6	
	MgO		3.5−110	9.8−Room temperature15.6	[28]
	SiO_2	800	8.6	9.3	[34]
	Al_2O_3	600	6.4	11.3	[35]
	Al_2O_3	600	4.4	11.3	[36]

placed on a 3 mm sapphire wafer, that insulates the sample from the heater, and is clamped by carbon contacts, to which voltage is applied via current leads. The current lead is insulated by ceramic couplings from other holder components. The sample is clamped on the sapphire insulator surface. The holder is secured in the system using threaded connection on magnetic leads that allow vertical movement along the whole height of the system, and is additionally retained between the mask and holder guides by wheels placed symmetrically on all sides of the housing.

To monitor temperature distribution and wafer heating conditions of each of the holders, separate measurements were performed. The holder was placed in a separate vacuum chamber, the pressure in which was maintained at $8 \cdot 10^{-7}$ Torr. A flange with a sight glass is provided in the chamber. ZnSe glass transparent in the wavelength range of $2 - 15\,\mu$m served as a sight glass material. The holder is placed so that its heating element is located directly in front of the glass (Figure 3, *a*). The heater is energized through vacuum bushings insulated from the housing. Temperature was monitored using the FLIR A-300 pyrometer every 5 min. For each of the heating modes, the required time to full heating and temperature distribution throughout the wafer area were measured.

Microstructure thickness, phase and chemical compositions of the grown films were measured using the FEI Titan 80−300 transmission electron microscope without spherical aberration corrector, with the Gatan GIF-2001 electron energy loss spectrometer. Accelerating voltage was 200 kV, spectrum recording parameters: electron beam convergence angle 10 mrad, detector collection angle 14.82 mrad, chamber length 60 mm, spectrometer aperture 3 mm. NbN/Al_2O_3 structure cross-sections were made using the FIB Helios Nanolab 650 focused ion beam system.

Quantitative analysis of element distribution through the depth of the deposited NbN film was performed in this study using the electron energy loss spectroscopy with converging beam (TSEM). This approach used on cross-section samples provided an element distribution profile throughout the film depth by a relative concentration

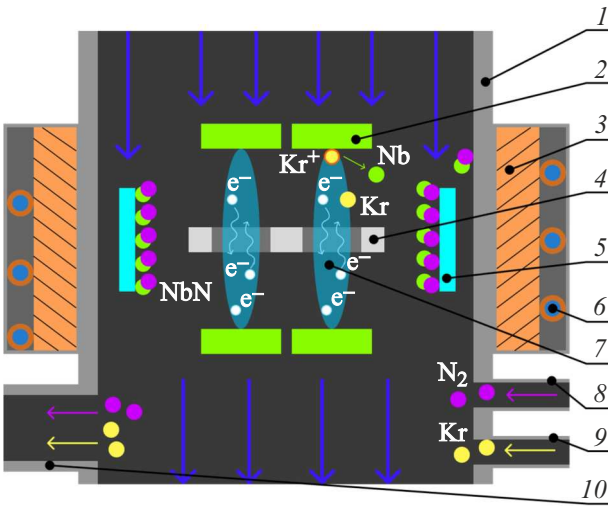

Figure 1. Schematic diagram of the UIR-11 sputtering system: *1* — vacuum chamber enclosure, *2* — cathode-targets (x4), *3* — solenoid, *4* — anode, *5* — wafer, *6* — solenoid cooling connections, *7* — plasma, *8* — nitrogen supply connection, *9* — krypton supply connection, *10* — pumping out connection.

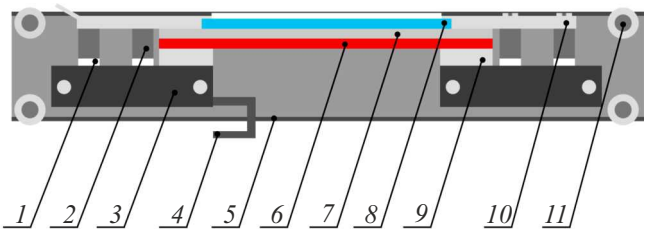

Figure 2. Schematic diagram of the sample holder with heater and wafer: *1* — ceramic insulator, *2* — supports, *3* — holder, *4* — current lead contact, *5* — carriage housing, *6* — silicon carbide heater, *7* — sapphire spacer, *8* — wafer sample, *9* — glass-graphite contacts, *10* — wafer sample clamps, *11* — carriage wheels.

method and made it possible to find the real thickness of the deposited film:

$$\frac{N_{\mathrm{Nb}}}{N_{\mathrm{N}}} = \frac{I_{\mathrm{Nb}}(\beta,\Delta)}{I_{\mathrm{N}}(\beta,\Delta)} \cdot \frac{\sigma_{\mathrm{N}}(\beta,\Delta)}{\sigma_{\mathrm{Nb}}(\beta,\Delta)}, \qquad (1)$$

where I_{Nb}, I_{N} are integral peak intensities under the niobium and nitrogen absorption curves after background subtraction, and σ_{Nb} and σ_{N} are cross-sections of inelastic scattering of Nb and N atoms for the given spectrometer collection angle β.

Moreover, note that EELS (electron energy loss spectrum) was examined using a technique for elemental composition data processing in absorption edge overlapping conditions [38]. This technique was used to separate the Nb — $M_{3,2}$ and N — K lines and, consequently, to reduce the scatter of atomic concentrations for each element throughout the film depth.

Phase analysis used high resolution bright-field patterns by constructing Fourier transform from the region of interest in Digital Micrograph. Then, the Fourier transform pattern, being completely equivalent to microdiffraction from a selected grain, was used to measure interplanar spacings and angles between the reflection system. Database was used for phase identification. PDF-4 [39].

2. Experiment and results

This study has experimentally investigated superconducting 5.5 nm NbN films. For each of the heating modes, two films were prepared on two different sample holders in a single process. Sapphire wafers with dimensions of 15×14 mm and thickness of $460\,\mu$m were used as substrates. Film thickness was measured indirectly using the Amibios XP-2 stylus profiler, and by direct measurements using a transmission electron microscope (see below). For indirect measurements, 50–100 nm films were preliminary fabricated, then thicknesses were measured. Sputtering rate was equal to 0.8 nm/min. Initial pressure in the working chamber was $8.9 \cdot 10^{-8}$ Torr. Initial conditions were achieved by preheating the system to 180 °C. Partial pressures of the injected gas mixture (nitrogen and krypton) were $2.4 \cdot 10^{-5}$ and $3.8 \cdot 10^{-5}$ Torr (nitrogen equivalent), respectively. Voltage applied to cathodes was 3.5 kV with ion current for each of the modes equal to $2 \cdot 10^{-3}$ A. Preliminary cathode cleaning (using sputtering mode) during 10 min was performed. The sample holders were removed from the sputtering region during cleaning. Direct sputtering started 40 min after heating as shown in the curves (Figure 3, *c*). Film resistances per square in normal state at 10 K are listed in Table 2.

Electrophysical properties of films were measured in an immersion cryostat. Superconducting transition temperature T_C was determined from $R(T)$. Critical current density J_C was measured on square samples with dimensions of $20 \times 20\,\mu$m (Figure 4, *a*) at 4.2 K. Structures were formed by the photolithography and reactive ion etching method as described in [40]. To evaluate film properties dispersion over the area, measurements were performed on samples prepared in various parts of the film: in the center and on the edges (Figure 4, *a*).

For the grown films, dependences of T_C and J_C on the wafer temperature (during film deposition) were measured. The grown NbN films had the superconducting transition temperatures of 6.9–9.8 K, and critical current densities ranging within $1.12 - 3.5 \cdot 10^5$ A/cm^2 (Figure 5). Data scatter over the wafer area was max. 5 %–7 %, which generally corresponds to the wafer heater temperature scatter.

Structural investigations of films were also performed using analytical transmission electron microscopy methods, including high-resolution microscopy (HRTEM) and electron energy loss spectroscopy (EELS).

Figure 6 shows the Nb and N distribution profile over the depth of the original deposited film. Experimental relative concentrations of elements calculated from the

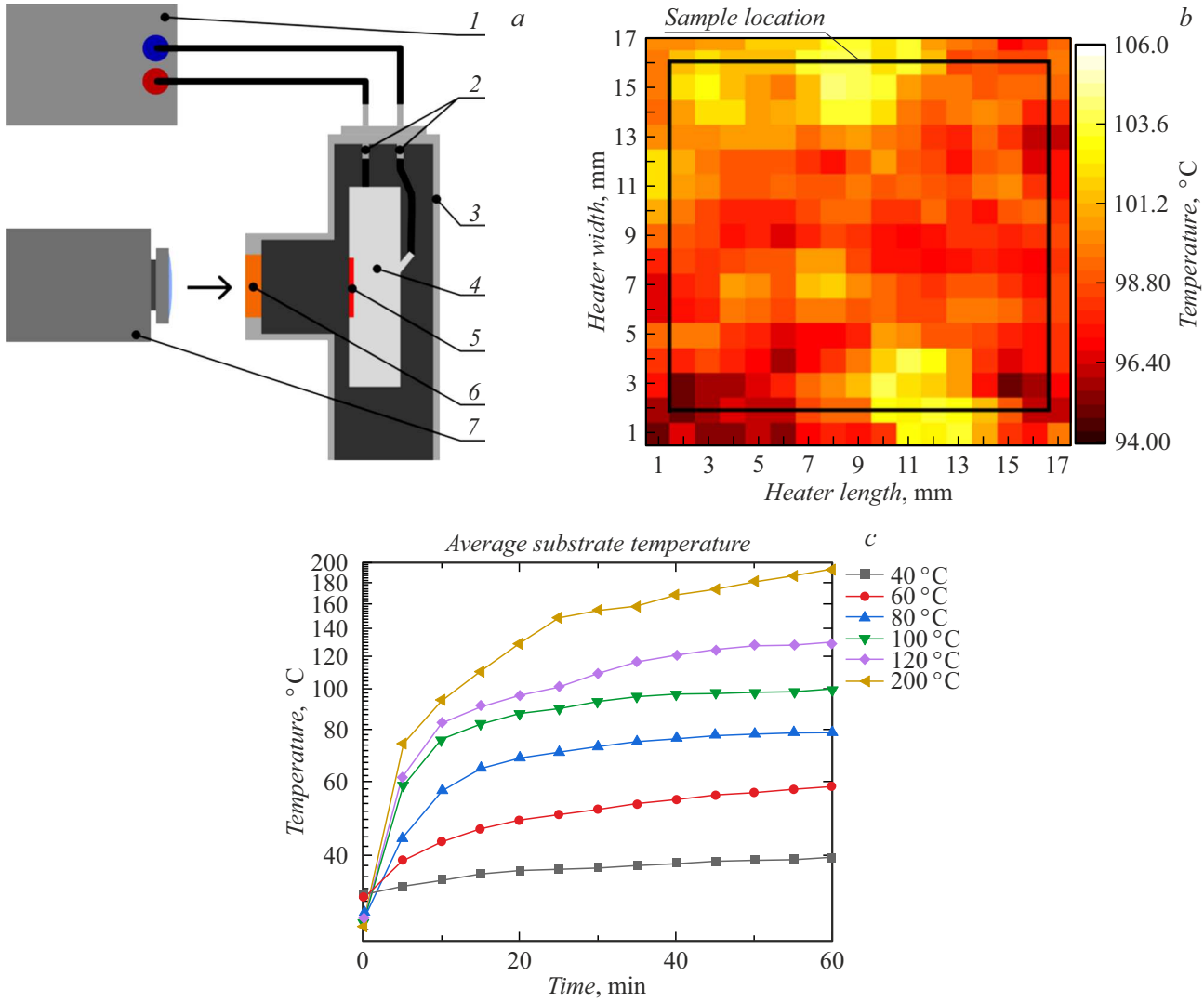

Figure 3. *a* — schematic diagram of wafer temperature measurements: *1* — power supply, *2* — current leads, *3* — vacuum chamber, *4* — sample holder, *5* — heater, *6* — ZnSe glass, *7* — thermal imager; *b* — temperature distribution over the wafer heater with the specified sample location; *c* — wafer heating curves.

Table 2. Resistances per square for films grown at different wafer temperatures

T wafer, °C	20	40	60	80	100	120
$R_{\square}$ at $T = 4.2$ K, Ω/□	560 ± 60	510 ± 60	580 ± 60	520 ± 50	450 ± 50	330 ± 30

electron energy loss spectra using a relative concentration method are shown by dots. It can be seen from the element distribution over the depth that the film has a homogeneous composition through the full depth, chemical composition corresponds to $Nb_{50}N_{50}$ taking into account the measurement error at each point at 0.5 nm intervals over the depth.

Thickness of the deposited films was evaluated using the transmission electron microscope on cross-section samples prepared by a focused ion beam (FIB) method. The high-resolution bright-field pattern (Figure 7, *a*) shows the structure of NbN film deposited on a Al_2O_3 single-crystal substrate. A protective Pt layer is deposited on top of the film during FIB preparation of cross-sections. The NbN film thickness may be evaluated taking into account the interface between the NbN film and Pt layers, and Al_2O_3 substrate, and according to the scale bar, and is equal to 5.5 nm. The NbN film is highlighted with a red frame in Figure 7, *a*. Microstructure of films deposited on Pt-coated Al_2O_3 single-crystal substrates is shown in Figure 7. The niobium nitride film is a 5.5 nm polycrystalline film with a grain size of ~ 3 nm. The high-resolution bright-

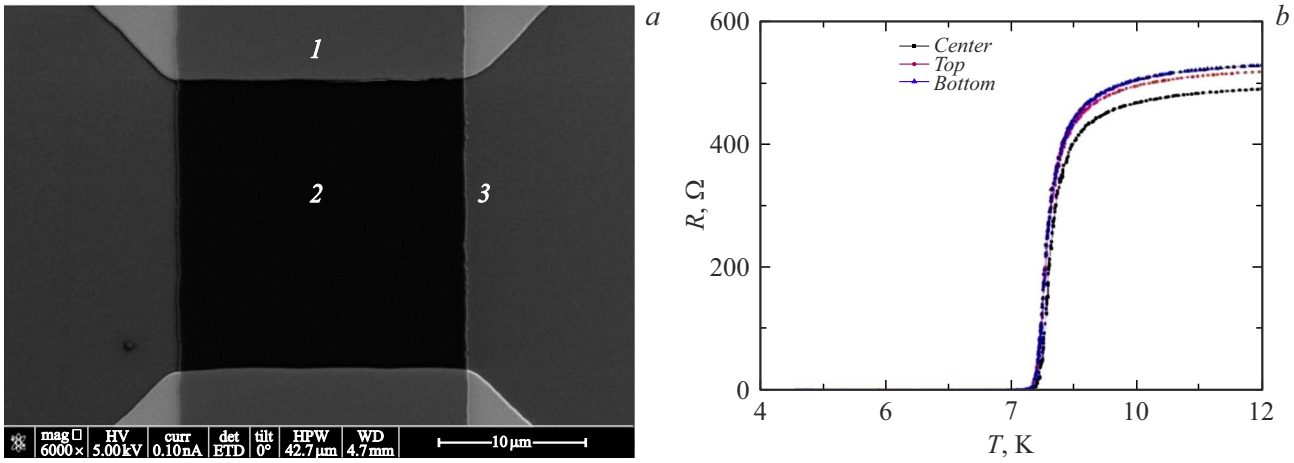

Figure 4. *a* — SEM image of a microbridge type sample with metallization contacts: *1* — metallization Pt contacts; *2* — 5.5 nm NbN film; *3* — sapphire wafer; *b* — measured $R(T)$ for samples from various points on the same NbN plate.

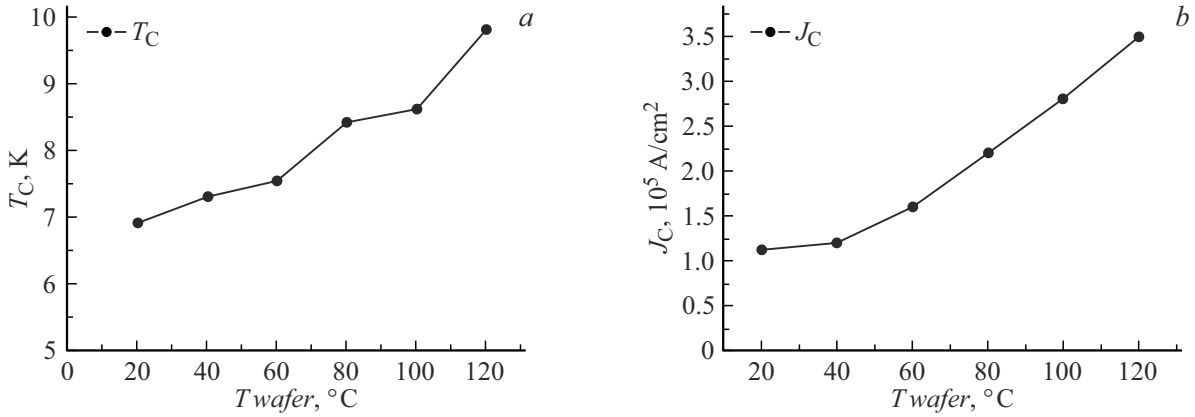

Figure 5. The temperature of film transition from normal to superconducting state T_C (a) and critical current density J_C (b) vs. the wafer temperature during deposition.

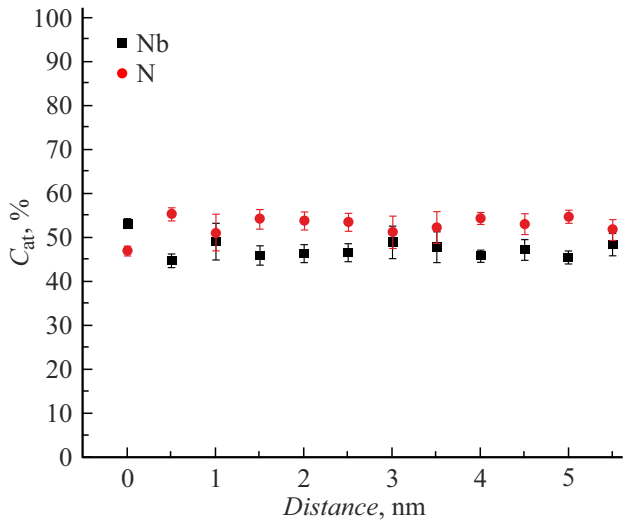

Figure 6. Nb and N atomic concentration distribution profile measured over the film thickness by the EELS method.

field image of the film cross-section was used to determine the phase composition. A grain region, from which the Fourier transform was obtained, is highlighted by a red square.

According to the results of transmission electron microscopy, the deposited films have the NbN composition with the zone axis $[0\bar{1}1]$ in the cubic crystal system Fm3m with the lattice parameter $a = 0.4394$ nm.

Analysis of the obtained data has shown that the NbN films fabricated in the given wafer temperature range has phase and elemental compositions corresponding to the NbN cubic phase.

Conclusion

The described cathode sputtering technique for ultrathin NbN film deposition is suitable for producing films with desired properties and is also applicable to cryoelectronic devices. The developed method for monitoring the wafer temperature and wafer temperature distribution during

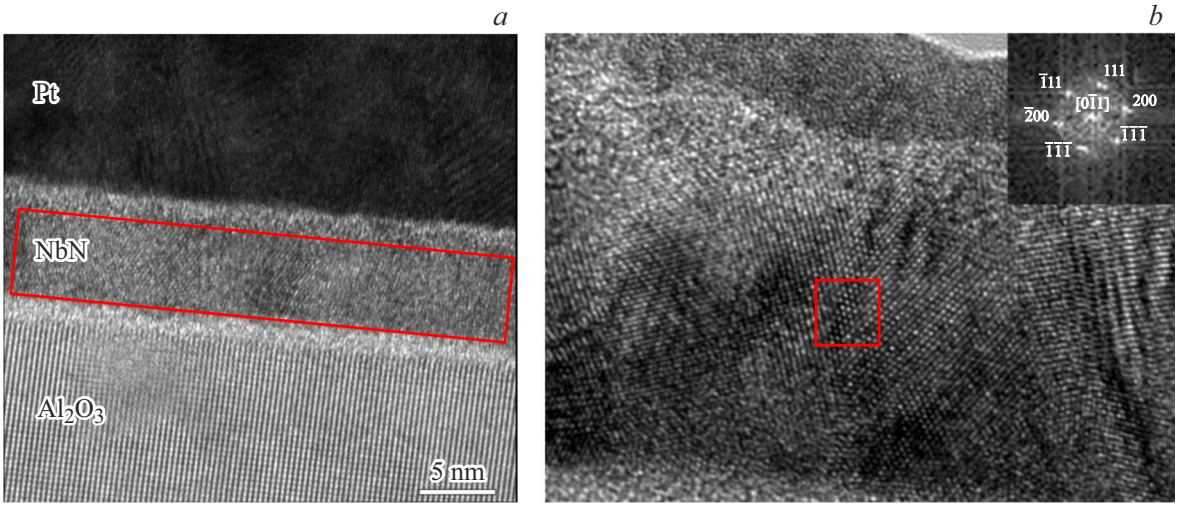

Figure 7. TEM high-resolution bright-field cross-section image of a polycrystalline NbN film sample on a single-crystal sapphire wafer: *a* — general view; *b* — phase analysis, inset — diffraction.

heating provides high uniformity of NbN properties over the area (the scatter is 5%–7%). Special focus shall be made on the possibility of producing multilayer structures and heterostructures due to the absence of annealing for making each successive layer because the wafer temperature range actually avoids diffusion processes and has almost no effect on the protective masks. The ultrathin NbN films deposited using the cathode sputtering technique have relatively high superconducting properties (T_C, J_C). Dependence of film properties on the wafer temperature. For the given temperature range, uniform wafer heating is critical because a temperature variation by 10 °C leads to significant modifications of final film properties. Note that the method proposed in the work has no fundamental limitations for ultrathin film deposition onto much larger wafers (100 mm in diameter), though will require structural modifications of the system. The work in this area will be continued.

Funding

This study was carried out under the state assignment of the National Research Center „Kurchatov Institute.“

Conflict of interest

The authors declare no conflict of interest.

References

[1] A.D. Semenov, G.N. Gol'tsman, A.A. Korneev. Physica C, **351**, 349 (2001). DOI: 10.1016/S0921- 4534(00)01637-3
[2] I.A. Stepanov, A.S. Baburin, D.V. Kushnev, E.V. Sergeev, O.I. Shmonina, A.R. Matanin, V.V. Echeistov, I.A. Ryzhikov, Yu.V. Panfilov, I.A. Rodionov. APL Mater., **12**, 021127 (2024). DOI: 10.1063/5.0188420
[3] H. Shi, T. Xu, Yi. Zhe, R. Su, J. Li, H. Bao, X. Tu, K. Fan, X. Jia, L. Kang, J. Chen, P. Wu. Appl. Phys. Lett., **126**, 042601 (2025). DOI: 10.1063/5.0231315
[4] I. Tretyakov, S. Ryabchun, M. Finkel, A. Maslennikova, N. Kaurova, A. Lobastova, B. Voronov, G. Gol'tsman. Appl. Phys. Lett., **98**, 033507 (2011). DOI: 10.1063/1.3544050
[5] A.N. McCaughan, K.K. Berggren. Nano Lett., **14**, 10, 5748 (2014). DOI: 10.1021/nl502629x
[6] B.A. Gurovich, K.E. Prikhodko, L.V. Kutuzov, B.V. Goncharov, D.A. Komarov, E.M. Malieva. FTT, **64** (10), 1390 (2022) (in Russian). DOI: 10.21883/FTT.2022.10.53079.47HH
[7] B.A. Gurovich, K.E. Prikhodko, L.V. Kutuzov, B.V. Goncharov. FTT, **62** (9), 1420 (2020). DOI: 10.21883/FTT.2020.09.49764.23H
[8] Q. Zhang, H. Wang, X. Tang, H. Xue, W. Peng, Zh. Wang. IEEE Transactions Appl. Superconduct., **28** (8), 1100704 (2018). DOI: 10.1109/tasc.2018.2869803
[9] Z. Wang, H. Terai, W. Qiu, K. Makise, Y. Uzawa, K. Kimoto, Y. Nakamura. Appl. Phys. Lett., **102**, 142604 (2013). DOI: 10.1063/1.4801972
[10] M. Ukibe, G. Fujii. IEEE Transactions Appl. Superconduct., **27** (4), 1051 (2016). DOI: 10.1109/TASC.2017.2655719
[11] M.J. Sowa, Y. Yemane, J. Zhang, J.C. Palmstrom, L. Ju, N.C. Strandwitz, F.B. Prinz, J. Provine. J. Vac. Sci. Technol. A, **35**, 01B143 (2017). DOI: 10.1116/1.4972858
[12] R. Cheng, S. Wang, H.X. Tang. Appl. Phys. Lett., **115**, 241101 (2019). DOI: 10.1063/1.5131664
[13] C. Sheagren, P. Barry, E. Shirokof, Q.Y. Tang. J. Low Temp. Phys., **199**, 875 (2020). DOI: 10.1007/s10909-020-02336-2
[14] M. Ziegler, S. Linzen, S. Goerke, U. Bruckner, J. Plentz, J. Dellith, A. Himmerlich, M. Himmerlich, U. Hubner, S. Krischok, H.-G. Meyer. IEEE Transactions Appl. Superconduct., **27** (7), 1 (2017). DOI: 10.1109/tasc.2017.2744326
[15] M.V.Shibalov, A.A.Shibalova, A.R.Shevchenko, A.M.Mumlyakov, I.A.Filippov, M.A.Tarkhov. ZhTF, **95** (1), 84 (2025) (in Russian). DOI: 10.61011/JTF.2025.01.59463.183-24

[16] S. Linzen, M. Ziegler, O.V. Astafiev, M. Schmelz, U. Hubner, M. Diege, E. Il'ichev, H.-G. Meyer. Supercond. Sci. Technol., **30**, 035010 (2017). DOI: 10.1088/1361-6668/aa572a
[17] S. Volkov, M. Gregor, T. Roch, L. Satrapinskyy, B. Grancic, T. Fiantok, A. Plecenik. J. Electrical Engeneer., **70** (7S), 89 (2019). DOI: 10.2478/jee-2019?0047
[18] V. Boffa, U. Gambardella, V. Marotta, A. Morone, F. Murtas, S. Orlando, G.P. Parisi. Appl. Surf. Sci., **106**, 361 (1966). DOI: 10.1016/S0169-4332(96)00432-1
[19] M.A. Mamun, A.H. Farha, A.O. Er, Y. Ufuktepe, D. Gu, H.E. Elsayed-Ali, A.A. Elmustafa. Appl. Surf. Sci., **258** (10), 4308 (2012). DOI: 10.1016/j.apsusc.2011.12.089
[20] R.E. Treece, J.S. Horwitz, J.H. Claassen, D.B. Chrisey. Appl. Phys. Lett., **65**, 2860 (1994). DOI: 10.1063/1.112516
[21] F. Mercier, S. Coindeau, S. Lay, A. Crisci, M. Benz, Th. Encinas, R. Boichot, A. Mantoux, C. Jimenez, F. Weiss, E. Blanquet. Surf. Coat. Technol., **260**, 126 (2014). DOI: 10.1016/j.surfcoat.2014.08.084
[22] W. Słysz, M. Guziewicz, M. Borysiewicz, J.Z. Domagaıa, I. Pasternak, K. Hejduk, W. Rzodkiewicz, J. Ratajczak, J. Bar, M. Węgrzecki, P. Grabiec, R. Grodecki, I. Węgrzecka, R. Sobolewski. Acta Phys. Polonica, Series a, **120** (1), 200 (2011). DOI: 10.12693/APhysPolA.120.200
[23] D. Hazra, N. Tsavdaris, S. Jebari, A. Grimm, F. Blanchet, F. Mercier, E. Blanquet, C. Chapelier, M. Hofheinz. Supercond. Sci. Technol., **29**, 105011 (2016). DOI: 10.1088/0953-2048/29/10/105011
[24] R.E. de Lamaestre, Ph. Odier, E. Bellet-Amalric, P. Cavalier, S. Pouget, J.-C. Villégier. J. Phys.: Conf. Ser., **97**, 012046 (2008). DOI: 10.1088/1742-6596/97/1/012046
[25] J.-C. Villegier, S. Bouat, P. Cavalier, R. Setzu, R.E. de Lamaëstre, C. Jorel, P. Odier, B. Guillet, L. Mechin, M.P. Chauvat, P. Ruterana. IEEE Transactions Appl. Superconduct., **19** (3), 3375 (2009). DOI: 10.1109/TASC.2009.2019
[26] J.R. Gao, M. Hajenius, F.D. Tichelaar, T.M. Klapwijk, B. Voronov, E. Grishin, G. Gol'tsman, C.A. Zorman, M. Mehregany. Appl. Phys. Lett., **91**, 062504 (2007). DOI: 10.1063/1.2766963
[27] F. Marsili, D. Bitauld, A. Fiore, A. Gaggero, F. Mattioli, R. Leoni, M. Benkahoul, F. Levy. Opt. Express, **16** (5), 3191 (2008). DOI: 10.1364/OE.16.003191
[28] Sh. Miki, M. Fujiwara, M. Sasaki, Zh. Wang. IEEE Transactions Appl. Superconduct., **17** (2), 285 (2007). DOI: 10.1109/TASC.2007.898582
[29] R. Baskaran, A.V. Thanikai Arasu, E.P. Amaladass, M.P. Janawadkar. J. Appl. Phys., **116**, 163908 (2014). DOI: 10.1063/1.4900436
[30] Z. Yang, X. Wei, P. Roy, D. Zhang, P. Lu, S. Dhole, H. Wang, N. Cucciniello, N. Patibandla, Zh. Chen, H. Zeng, Q. Jia, M. Zhu. Materials, **16**, 7468 (2003). DOI: 10.3390/ ma16237468
[31] E.I. Alessandrini, V. Sadagopan, R.B. Laibowitz. J. Vacuum Sci. Technol., **8**, 188 (1971). DOI: 10.1116/1.1316283
[32] K. Buttig, H. Liemersdorf, H. Kinder, K. Reichelt. J. Appl. Phys., **44**, 5069 (1973). DOI: 10.1063/1.1662091
[33] H.-J. Hedbabny, H. Rogalla. J. Appl. Phys., **63**, 2086 (1988). DOI: 10.1063/1.341113
[34] D. Dochev, V. Desmaris, A. Pavolotsky, D. Meledin, Z. Lai, A. Henry, E. Janzen, E. Pippe, J. Woltersdorf, V. Belitsky. Supercond. Sci. Technol., **24**, 035016 (2011). DOI: 10.1088/0953-2048/24/3/035016
[35] P. Feautrier, E. le Coarer, R.E. de Lamaestre, P. Cavalier, L. Maingault, J.C. Villégier, L. Frey, J. Claudon, N. Bergeard, M. Tarkhov, J.-P. Poizat. J. Phys.: Conf. Ser., **97**, 012087 (2008). DOI: 10.1088/1742-6596/97/1/012087
[36] R.E. de Lamaéstre, Ph. Odier, J.-C. Villégier. Appl. Phys. Lett., **91**, 232501 (2007). DOI: 10.1063/1.2820607
[37] D.I. Dolgii, E.D. Ol'shanskii, E.P. Ryazantsev. Konversiya v mashinostroenii, 3–4, 119 (1999) (in Russian).
[38] K.E. Prikhodko, M.M. Dementieva. ZhTF, 94 (8), 1314 (2024). (in Russian)
[39] D.B. Williams, C.B. Carter. *Transmission Electron Microscopy: A Textbook for Materials Science* (Springer, 2009)
[40] B.A. Gurovich, K.E. Prikhod'ko, M.A. Tarkhov, E.A. Kuleshova, D.A. Komarov, V.L. Stolyarov, E.D. Ol'shanskii, B.V. Goncharov, D.A. Goncharova, L.V. Kutuzov, A.G. Domantovskii, Z.V. Lavrukhina, M.M. Dement'eva. Nanotechnol. Russ., **10** (7-8), 530 (2015). DOI: 10.1134/S1995078015040072

Translated by E.Ilinskaya